Supplement of Geosci. Model Dev., 15, 5883–5903, 2022
https://doi.org/10.5194/gmd-15-5883-2022-supplement

Geoscientific
Model Development

Supplement of

TransClim (v1.0): a chemistry–climate response model for assessing the effect of mitigation strategies for road traffic on ozone

Vanessa Simone Rieger and Volker Grewe

Correspondence to: Vanessa Simone Rieger (vanessa.rieger@dlr.de)

SI-text: OA source apportionment

OA source apportionment was performed on high resolution mass spectra for *m/z* 12-120 using PMF combined with the multilinear engine (ME-2) in Igor Pro (Paatero, 1999; Canonaco et al., 2013). First, a range of solutions with two to ten factors from unconstrained runs were examined. The OA factors are mixed with each other seriously in less factor number solutions, and increasing the number of factors can improve the separation. As shown in Fig. S4, four POA factors including HOA, COA, CCOA and BBOA were resolved in the 6-factor solution, while high signal of CO_2^+ was mixed in CCOA and COA factors. Meanwhile, two SOA factors with different oxidation states were also resolved, referred to as LO-OOA with O/C ratio of 0.42 and MO-OOA with O/C ratio of 1.02, respectively. However, much hydrocarbon-like ions in higher *m/z* were observed in LO-OOA, also suggesting the mixture between POA factors and SOA factors. In seven factors solution, the mixture of CO_2^+ in COA was reduced, while the mixture in CCOA and LO-OOA were still observed, and MO-OOA was separated into MO-OOA1 and MO-OOA2. When further increasing the factor into eight, clear POA sources including CCOA, BBOA, COA, and HOA were resolved. and the mixture in LO-OOA was also reduced. However, the MO-OOA is still separated into MO-OOA1 and MO-OOA2, and there was no new meaningful factor resolved. Therefore, six sources including HOA, COA, CCOA, BBOA, LO-OOA and MO-OOA should be resolved. Note that reasonable POA sources could not be resolved in six PMF solution, while SOA was separated in the seven and eight factor solutions. To optimize the source apportionment, we further conducted 6-factor solution using ME-2 approach in order to obtain a more environmentally meaningful result (Canonaco et al., 2013). The clear profiles of HOA, COA, CCOA and BBOA resolved in 8-factor PMF solution were used to constrain these four sources, and a-value of 0.1 was applied for a reasonable variation range. Finally, six OA sources including HOA, COA, BBOA, CCOA, LO-OOA, and MO-OOA were identified (Fig. S5).

As for POAs, both the mass spectrum of HOA and COA are characterized by prominent hydrocarbon ion series of C_nH_{2n-1} and C_nH_{2n+1}, while the COA contains higher signal at C_nH_{2n-1} than C_nH_{2n+1}, an especially much higher signal ratio of $C_4H_7^+/C_4H_9^+$ which is the typical characteristic of COA profile as reported in previous studies at various urban sites (He et al., 2011; Ng et al., 2011). The HOA was emitted mainly from local traffic with mass peaks in traffic hours (Huang et al., 2010; Sun et al., 2011; Ge et al., 2012), and COA was dominantly associated with the cooking emissions (He et al., 2010; Xu et al., 2016), exhibiting mass peaks at around breakfast, lunch and dinner times (Fig. S6). Meanwhile, the time series of COA correlated well with that of $C_6H_{10}O^+$ (r=0.85), which is a tracer fragment of cooking emissions (Sun et al., 2011; Hu et al., 2016) (Fig. S6). The mass spectrum of CCOA is dominated by unsaturated hydrocarbons, particularly polycyclic aromatic hydrocarbons (PAH)-related ion peaks (e.g., *m/z* 77, 91 and 115) (Dall'Osto et al., 2013; Hu et al., 2013). In comparison, BBOA was mainly emitted from the combustion of biomass fuel such as wood or straw (Wang et al., 2009; Zhang et al., 2015), with the tracer signal at *m/z* 60 (dominantly $C_2H_4O_2^+$), which is mainly enhanced by biomass-burning tracer levoglucosan and related species (mannosan, galactosan, etc.) (Cubison et al., 2011). Consistently, a good correlation between the time series of BBOA and the $C_2H_4O_2^+$ fragment was also observed (r=0.95) (Fig. S6).

As for SOAs, the mass spectrum of LO-OOA shows a higher peak at *m/z* 43 (mainly $C_2H_3O^+$) and a lower O/C ratio (0.57) than that of MO-OOA (0.82). The tight correlation between the time series of $C_2H_3O^+$ and LO-OOA ($r = 0.83$) also suggests its less oxidized property (Fig. S6). In addition, obvious *m/z* 60 ($C_2H_4O_2^+$) and *m/z* 73 ($C_3H_5O_2^+$) peaks were found in the mass spectrum of LO-OOA and the time variation of LO-OOA correlated well with that of BBOA (R^2=0.59) (Fig. S7), suggesting the possible influence of BBOA source on the formation of LO-OOA. Therefore, LO-OOA was further referred to as OOA-BB and discussed in detail in section 3.2. In comparison, MO-OOA has a mass spectrum with a much higher peak at *m/z* 44 (mainly CO_2^+) than *m/z* 43, and a largely different time series with LO-OOA, implying different formation processes. Meanwhile, the time series of MO-OOA was correlated well with the typical fragment ions of aqueous-phase processing products including $CH_2O_2^+$ ($R^2 = 0.91$), CH_3SO^+ ($R^2 = 0.89$), and $CH_3SO_2^+$ ($R^2 = 0.75$) (Fig. S8) (Tan et al., 2009; Chhabra et al., 2010; Ge et al., 2012; Sun et al., 2016), suggesting the dominant role of aqueous-phase processes in its formation. Therefore, MO-OOA was further referred to as aq-OOA and discussed in detail in section 3.3.

Table S1 Summary of mass concentrations of NR-$PM_{2.5}$ species (μg m^{-3}), OA sources (μg m^{-3}), gaseous pollutants (μg m^{-3} for SO_2, NO_2, O_3, and mg m^{-3} for CO), ALWC (μg m^{-3}), meteorological parameters (RH, Temperature (T)) and elemental ratios (H/C, O/C) during different periods according to this study.

Species	**Entire study**	**reference**	**SIA-P1**	**SIA-P2**
NR-$PM_{2.5}$	68.0±42.8	44.1±25.5	131.0±49.6	84.9±30.7
OA	37.1±19.2	28.7±16.4	68.0±20.7	37.7±11.7
SO_4^{2-}	8.7±8.5	3.5±2.8	18.4±10.2	14.7±7.2
NO_3^-	13.3±11.4	6.8±4.9	27.4±13.4	19.9±9.3
NH_4^+	6.8±5.7	3.3±2.2	13.3±6.5	10.8±4.6
Cl^-	2.1±1.8	1.8±1.8	3.9±1.9	1.8±0.7
HOA	3.0±3.9	3.3±4.2	4.6±4.2	1.3±1.3
COA	4.8±4.2	4.8±4.4	7.0±4.8	3.5±2.3
CCOA	3.2±2.5	3.0±2.3	5.8±2.8	2.0±1.5
BBOA	4.3±5.9	3.9±5.6	9.6±7.7	2.1±2.6
OOA-BB	9.0±7.3	8.8±7.8	14.8±6.4	6.1±3.9
aq-OOA	12.8±12.6	4.9±3.7	26.2±14.6	22.7±10.7
SO_2	16.9±8.9	19.5±9.8	17.2±5.2	10.6±4.1
NO_2	64.4±25.4	64.8±26.2	82.8±18.9	52.2±19.5
O_3	30.0±26.7	28.6±25.8	16.3±12.4	41.9±30.1
CO	1.5±0.6	1.3±0.5	2.2±0.5	1.4±0.3
ALWC	38.8±69.7	12.8±66.8	90.4±104.5	73.7±84.3
RH (%)	58.1±22.0	50.3±20.4	67.9±19.6	70.4±18.7
T (°C)	1.4±5.9	1.7±6.0	-2.8±4.8	3.1±4.9
H/C	1.71±0.07	1.74±0.06	1.72±0.05	1.65±0.04
O/C	0.50±0.15	0.41±0.10	0.52±0.10	0.67±0.11

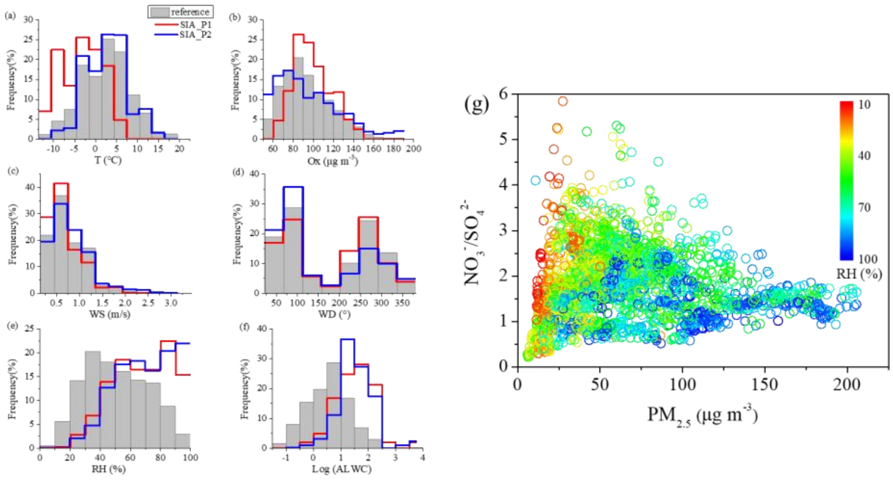

Fig. S1 Comparisons of frequencies of temperature(a), Ox concentration(b), WS(c), WD(d), RH(e) and ALWC(f) between reference days and SIA-enhanced periods (SIA_P1 and SIA_P2), and variation of NO_3^-/SO_4^{2-} ratio as a function of $PM_{2.5}$ mass, colored by RH during winter campaign (g).

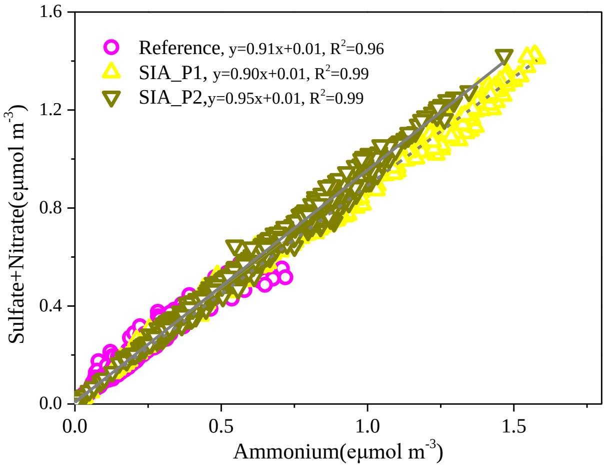

Fig. S2 Correlation between the equivalent molar concentration of ammonium and the sum of sulfate and nitrate during different periods (reference, SIA_P1, and SIA_P2) in winter Xi’an.

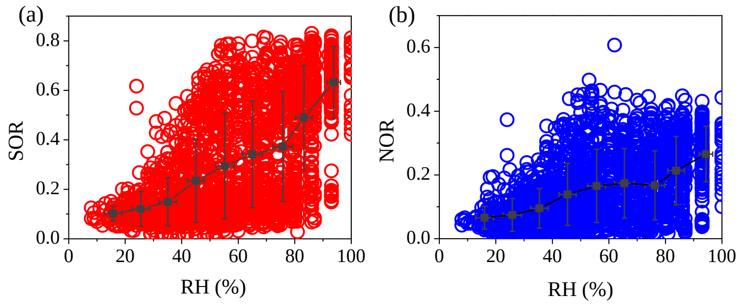

Fig. S3 Correlation between RH and SOR (a) or NOR (b) during the winter campaign in Xi'an.

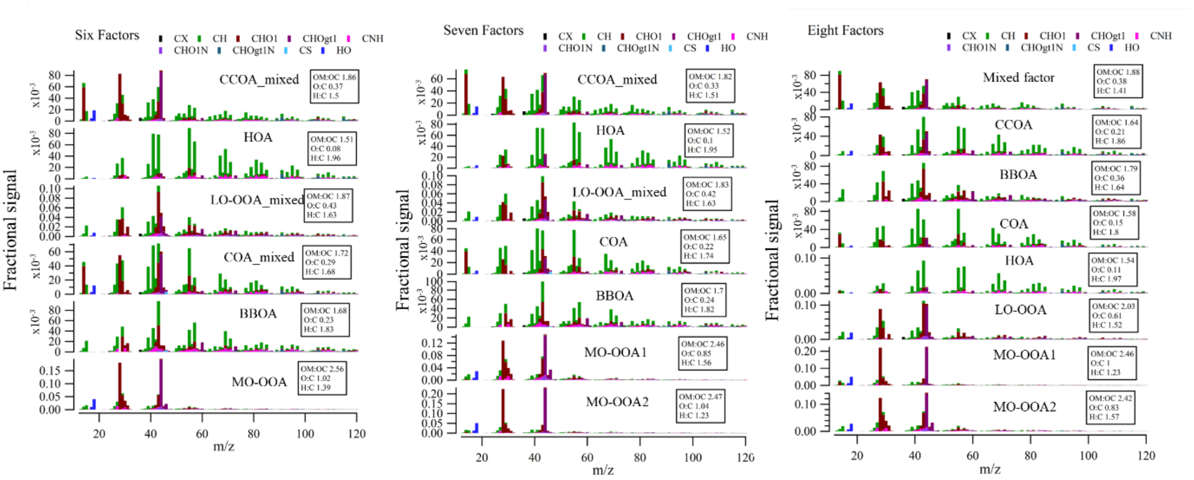

Fig. S4 Profiles (HR) of OA sources for six, seven and eight factors PMF solutions during the winter campaign in Xi'an.

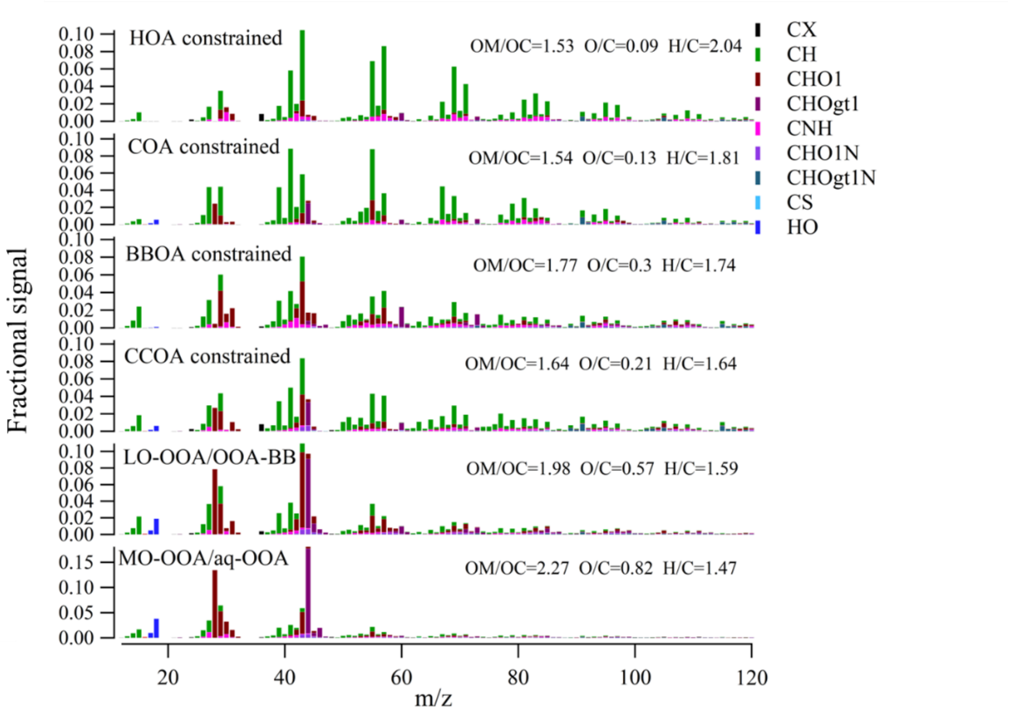

Fig. S5 Profiles (HR) of OA sources for six factors ME-2 solution during the winter campaign in Xi'an.

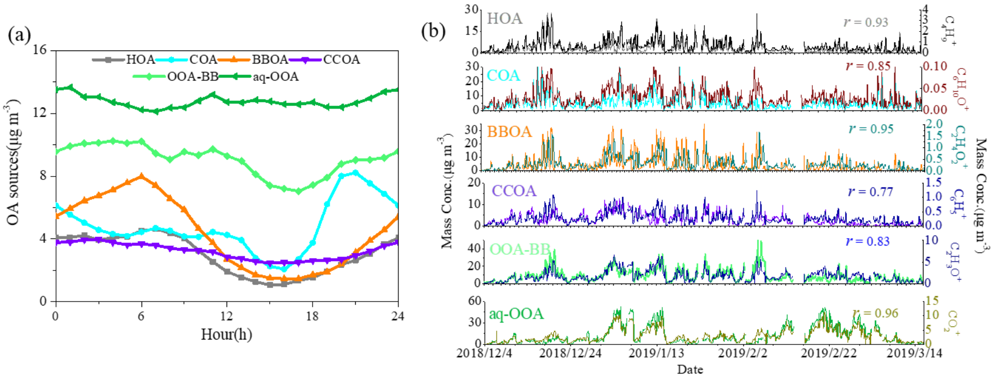

Fig. S6 Diurnal cycles of OA sources (a), and the time series of each source and their tracers during the winter campaign (b).

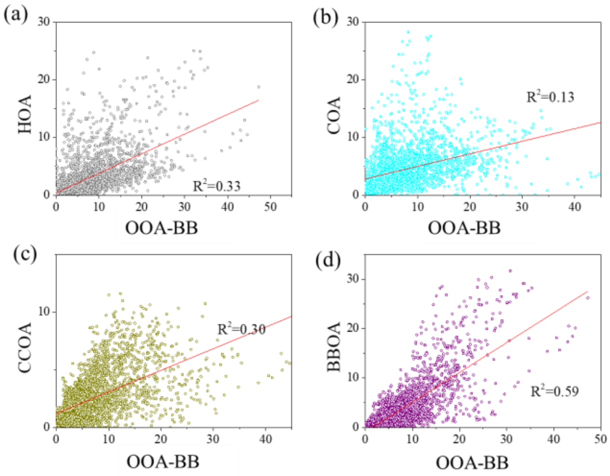

Fig. S7 Correlation between the concentration (μg m^{-3}) of OOA-BB and HOA (a), COA (b), CCOA (c) and BBOA (d).

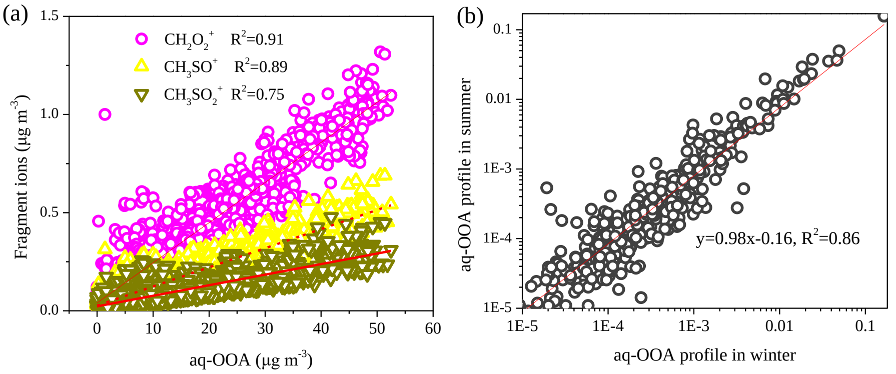

Fig. S8 Correlations between the concentration of aq-OOA and aqueous-phase processing fragment ions including $CH_2O_2^+$, CH_3SO^+, and $CH_3SO_2^+$ (a), and the correlation between the aq-OOA profile resolved in the winter campaign and the aq-OOA profile resolved in the summer of 2019 in Xi'an (b).

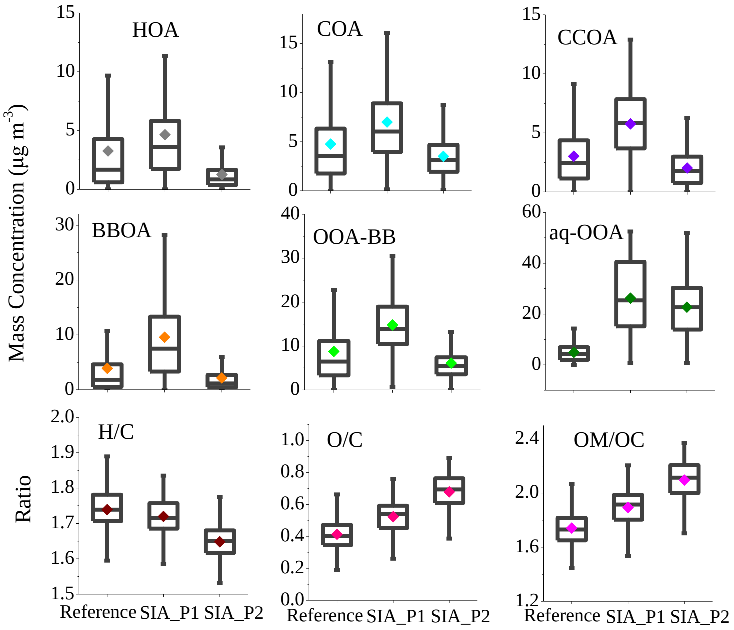

Fig. S9 Mass concentrations of OA sources, OA oxidation ratios (H/C, O/C and OM/OC) during different periods including reference days, SIA_P1 and SIA_P2.

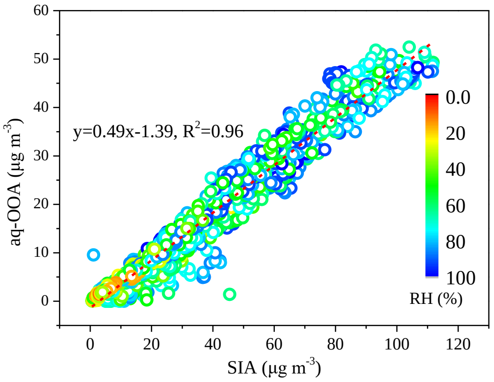

Fig. S10 Correlation between the concentration of aq-OOA and SIA during the entire winter campaign in Xi'an.

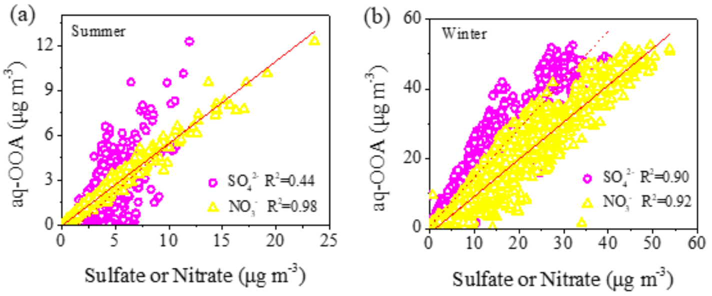

Fig. S11 Correlation between the concentration of aq-OOA and sulfate or nitrate during summer (a), and winter (b) in Xi'an.

Reference

Canonaco, F., Crippa, M., Slowik, J. G., Baltensperger, U., and Prévôt, A. S. H.: SoFi, an IGOR-based interface for the efficient use of the generalized multilinear engine (ME-2) for the source apportionment: ME-2 application to aerosol mass spectrometer data, Atmos. Meas. Tech., 6(12), 3649, https://doi.org/10.5194/amt-6-3649-2013, 2013.

Chhabra, P. S., Flagan, R. C., and Seinfeld, J. H.: Elemental analysis of chamber organic aerosol using an aerodyne high-resolution aerosol mass spectrometer, Atmos. Chem. Phys., 10, 4111–4131, https://doi.org/10.5194/acp-10-4111-2010, 2010.

Cubison, M. J., Ortega, A. M., Hayes, P. L., Farmer, D. K., Day, D., Lechner, M. J., Brune, W. H., Apel, E., Diskin, G. S., Fisher, J. A., Fuelberg, H. E., Hecobian, A., Knapp, D. J., Mikoviny, T., Riemer, D., Sachse, G. W., Sessions, W., Weber, R. J., Weinheimer, A. J., Wisthaler, A., and Jimenez, J. L.: Effects of aging on organic aerosol from open biomass burning smoke in aircraft and laboratory studies, Atmos. Chem. Phys., 11, 12049–12064, https://doi.org/10.5194/acp-11-12049-2011, 2011.

Dall'Osto, M., Ovadnevaite, J., Ceburnis, D., Martin, D., Healy, R. M., O'Connor, I. P., Kourtchev, I., Sodeau, J. R., Wenger, J. C., and O'Dowd, C.: Characterization of urban aerosol in Cork city (Ireland) using aerosol mass spectrometry, Atmos. Chem. Phys., 13, 4997–5015, https://doi.org/10.5194/acp-13-4997-2013, 2013.

Ge, X. L., Setyan, A., Sun, Y. L., and Zhang, Q.: Primary and secondary organic aerosols in Fresno, California during wintertime: Results from high resolution aerosol mass spectrometry, J. Geophys. Res., 117, D19301, https://doi.org/10.1029/2012JD018026, 2012.

He, L. Y., Lin, Y., Huang, X. F., Guo, S., Xue, L., Su, Q., Hu, M., Luan, S. J., and Zhang, Y. H.: Characterization of high-resolution aerosol mass spectra of primary organic aerosol emissions from Chinese cooking and biomass burning, Atmos. Chem. Phys., 10, 11535–11543, https://doi.org/10.5194/acp-10-11535-2010, 2010.

He, L. Y., Huang, X. F., Xue, L., Hu, M., Lin, Y., Zheng, J., Zhang, R. Y., and Zhang, Y. H.: Submicron aerosol analysis and organic source apportionment in an urban atmosphere in Pearl River Delta of China using high-resolution aerosol mass spectrometry, J. Geophys. Res., 116, D12304, https://doi.org/10.1029/2010JD014566, 2011.

Hu, W. W., Hu, M., Yuan, B., Jimenez, J. L., Tang, Q., Peng, J. F., Hu, W., Shao, M., Wang, M., Zeng, L. M., Wu, Y. S., Gong, Z. H., Huang, X. F., and He, L. Y.: Insights on organic aerosol aging and the influence of coal combustion at a regional receptor site of central eastern China, Atmos. Chem. Phys., 13, 10095–10112, https://doi.org/10.5194/acp-13-10095-2013, 2013.

Hu, W. W., Hu, M., Hu, W., Jimenez, J. L., Yuan, B., Chen, W., Wang, M., Wu, Y., Chen, C., Wang, Z., Peng, J., Zeng, L., and Shao, M.: Chemical composition, sources, and aging process of submicron aerosols in Beijing: Contrast between summer and winter, J. Geophys. Res.-Atmos., 121, 1955–1977, https://doi.org/10.1002/2015JD024020, 2016.

Huang, X.-F., He, L.-Y., Hu, M., Canagaratna, M. R., Sun, Y., Zhang, Q., Zhu, T., Xue, L., Zeng, L.-W., Liu, X.-G., Zhang, Y.-H., Jayne, J. T., Ng, N. L., and Worsnop, D. R.: Highly time-resolved chemical characterization of atmospheric submicron particles during 2008 Beijing Olympic Games using an Aerodyne High-Resolution Aerosol Mass Spectrometer, Atmos. Chem. Phys., 10, 8933–8945, https://doi.org/10.5194/acp-10-8933-2010, 2010.

Paatero, P.: The multilinear engine: a table-driven, least squares program for solving multilinear problems, including the n-way parallel factor analysis model, J. Comput. Graph. Stat., 8, 854–

888, https://doi.org/10.1080/10618600.1999.10474853, 1999.

Sun, Y.-L., Zhang, Q., Schwab, J. J., Demerjian, K. L., Chen, W.-N., Bae, M.-S., Hung, H.-M., Hogrefe, O., Frank, B., Rattigan, O. V., and Lin, Y.-C.: Characterization of the sources and processes of organic and inorganic aerosols in New York city with a high-resolution time-of-flight aerosol mass spectrometer, Atmos. Chem. Phys., 11, 1581–1602, https://doi.org/10.5194/acp-11-1581-2011, 2011.

Sun, Y. L., Du, W., Fu, P., Wang, Q., Li, J., Ge, X., Zhang, Q., Zhu, C., Ren, L., Xu, W., Zhao, J., Han, T., Worsnop, D. R., and Wang, Z.: Primary and secondary aerosols in Beijing in winter: sources, variations and processes, Atmos. Chem. Phys., 16, 8309–8329, https://doi.org/10.5194/acp-16-8309-2016, 2016.

Tan, Y., Perri, M. J., Seitzinger, S. P., and Turpin, B. J.: Effects of Precursor Concentration and Acidic Sulfate in Aqueous Glyoxal-OH Radical Oxidation and Implications for Secondary Organic Aerosol, Environ. Sci. Technol., 43, 8105–8112, https://doi.org/10.1021/es901742f, 2009.

Wang, Q., Shao, M., Zhang, Y., Wei, Y., Hu, M., and Guo, S.: Source apportionment of fine organic aerosols in Beijing, Atmos. Chem. Phys., 9, 8573–8585, https://doi.org/10.5194/acp-9-8573-2009, 2009.

Xu, J., Shi, J., Zhang, Q., Ge, X., Canonaco, F., Prévôt, A. S. H., Vonwiller, M., Szidat, S., Ge, J., Ma, J., An, Y., Kang, S., and Qin, D.: Wintertime organic and inorganic aerosols in Lanzhou, China: sources, processes, and comparison with the results during summer, Atmos. Chem. Phys., 16, 14937–14957, https://doi.org/10.5194/acp-16-14937-2016, 2016.

Zhang, J. K., Wang, Y. S., Huang, X. J., Liu, Z. R., Ji, D. S., and Sun, Y.: Characterization of organic aerosols in Beijing using an aerodyne high-resolution aerosol mass spectrometer, Adv. Atmos. Sci., 32, 877–888, https://doi.org/10.1007/s00376-014-4153-9, 2015.